Supporting Information

Gavriljuk et al. 10.1073/pnas.1307655110

SI Materials and Methods

Protein Expression and Purification. Bovine GDP dissociation inhibitor 1 (GDI-1) and the guanine nucleotide exchange factor (GEF) domain of human Connecdenn 1 were kindly provided by L. Oesterlin and N. Bleimling (Max-Planck-Institute for Molecular Physiology, Dortmund, Germany), and were prepared as described elsewhere (1, 2). His_6-MBP-Rab35 and His_6-MBP-Rab1b containing the C-terminal CAAX-box [Rab35CVIL and Rab1bCVIL (1)], His_6-AnkX (2), His_6-GST-GGTase I α and His_6-GGTase I β (1), His_6-GST-RabGGTase β (3), His_6-$TBC1D20_{1–362}$ (4), and His_6-GDI from *Saccharomyces cerevisiae* (5) were expressed in *Escherichia coli* BL21 DE3 RIL overnight at 18 °C induced by 0.2 mM isopropyl β-D-1-thiogalactopyranoside. The subunits of GGTase I were coexpressed and copurified. Rab1b with the C terminus of Rab35 consisted of $Rab1b_{1–176}$ and $Rab35_{176–199CVIL}$ and was expressed in the same manner. All constructs had a TEV protease cleavage site for tag removal, with the exception of GGTase I β, which had a thrombin site.

A two-step purification protocol was used to purify the proteins. Nickel affinity chromatography was performed on NiNTA Superflow (Qiagen) in the first purification step, followed by proteolytic tag removal and size exclusion chromatography on HiLoad 26/60 Superdex 75. Columns were provided by GE Life Sciences. In principle, buffer conditions were the same for all proteins, with notable exceptions given below. For nickel affinity chromatography, 50 mM NaP_i, pH 8, 300 mM NaCl, and 1 mM β-mercaptoethanol were used. For gel filtration, 50 mM Hepes, pH 7.5, 50 mM NaCl, and 2.5 mM dithioerythreitol were used. GTPases were supplemented with 2 mM $MgCl_2$ and 20 μM GDP. For Rab35 and Rab1b with the C terminus of Rab35, NaCl was raised to 200 mM and 5% glycerol was included, additionally. For AnkX, NaCl was raised to 200 mM as well. GGTase I was supplemented with 2 mM $MgCl_2$.

Preparative Geranylgeranylation. Geranylgeranyl pyrophosphate was purchased from Sigma-Aldrich, and the reaction was directly carried out in the provided glass vials. It had to be considered that a vial contained ∼460 nmol of geranylgeranyl pyrophosphate, limiting the amount of protein to be prenylated. Also, methanol contained in the vial should not exceed 5 vol% in the final reaction mixture. Therefore, the final reaction volume was set to 3 mL, containing 5 mg of the GTPase with 5 mol% of GGTase I in the following buffer: 50 mM Hepes, pH 7.5, 50 mM NaCl, 2 mM $MgCl_2$, 2.5 mM dithioerythreitol, 20 μM GDP, 2% (wt/vol) CHAPS, 10% (wt/vol) glycerol, and 10 μM $ZnSO_4$. The mixture was incubated overnight at 8 °C with slight agitation. The products were separated by gel filtration on HiLoad 16/60 Superdex 75 (GE Life Sciences) in the same buffer with CHAPS reduced to 0.5% (wt/vol) and without glycerol and zinc chloride. Prenylated protein was concentrated (Amicon Ultra concentrators; Millipore) and RabGGTase β was added in a 1:1 molar ratio. To remove detergent, the buffer was exchanged with a NAP5 column (GE Life Sciences) to the same buffer without CHAPS, and any residual detergent was removed with a detergent removal spin column (Thermo Scientific). The resulting complex was analyzed by MALDI-MS to verify the prenylation (Fig. S6*A*).

Preparative Phosphocholination. Rab35 could be conveniently phosphocholinated before geranylgeranylation. Usually, 7 mg of Rab35 were incubated with 2 mol% AnkX and 2 mM CDP-choline (Sigma-Aldrich) for 3 h at room temperature in the following buffer: 50 mM Hepes, pH 7.5, 200 mM NaCl, 2 mM $MgCl_2$, 2.5 mM dithioerythreitol, 20 μM GDP, and 5% (vol/vol) glycerol. Products were separated by gel filtration and phosphocholination was verified by ESI-MS (Fig. S6*B*).

ATR Crystal Preparation. We closely follow the procedure described elsewhere (6). In short, the germanium crystal was polished by machine (Logitech CP50, 0.1 μM diamond polishing suspension, Microtex 500 HC-W polishing cloth, Logitech) and rinsed with deionized water. Hydrophilicity of the crystal was attained by 10-min incubation in concentrated sulfuric acid. After rinsing with water, the crystal was treated with air plasma (Harrick Scientific) for 10 min to further increase hydrophilicity and remove potential organic contaminants. In addition to this procedure, we found it useful to perform a manual polishing step before the incubation in sulfuric acid using 0.1 μM polishing paste (Sommer Präzisionstechnik) and a soft paper tissue.

Preparation of Small Unilamellar Vesicles. A total of 1.64 μmol of 1,2-dioleoyl-*sn*-glycero-3-phosphocholine (DOPC) and 1,2-dioleoyl-*sn*-glycero-3-phospho-L-serine (DOPS) (Avanti Polar Lipids) were mixed in a 9:1 molar ratio in 50 μL of chloroform. Chloroform was then removed under mild nitrogen flow and subsequent incubation in vacuum for 1 h. The lipids were resuspended in 200 μL of buffer (10 mM Tris, pH 7.5, 5 mM $MgCl_2$) by shaking at 37 °C and 1,200 rpm for 1 h in a thermomixer. Additionally, the lipids were vortexed every 15 min during this incubation. The resulting suspension was sonicated (Branson W-250 D cup sonifier; Heinemann) for 15 min with ice bath cooling. Any remaining multilamellar vesicles were removed by centrifugation at 13,000 × *g* for 15 min at 8 °C.

Attenuated Total Reflection Measurements. Attenuated total reflection (ATR)–Fourier transform infrared spectroscopy measurements were performed with a Vertex 80V spectrometer (Bruker Optik) at 293 K, with a spectral resolution of 2 cm^{-1} and a scanner velocity of 80 kHz. Scans were performed in the double-sided forward–backward mode with Blackman–Harris three-term apodization and a zero filling of 4. A vertical ATR multireflection unit (Specac) was used. The internal reflection element (IRE) was a 52 mm × 20 mm × 2 mm trapezoidal germanium ATR plate (ACM or Korth Kristalle) with an aperture angle of 45°. Only one side of the IRE was used, which resulted in 13 active reflections. Solutions were passed over the IRE at a flow rate of 1 mL/min by means of a peristaltic pump.

For vesicle spreading, 100 μL of vesicle solution (see above) were circulated in a total volume of 2.5 mL (10 mM Tris, pH 7.5, 5 mM $MgCl_2$) over the IRE until a stable lipid bilayer was formed. The bilayer was shortly flushed with water and then washed with buffer. Layer completeness was verified with 50 μg of BSA, which binds to germanium but not to a lipid bilayer (7). For characterization of the lipid bilayer, see below.

To bind Rab GTPases to the bilayer, geranylgeranylated Rab proteins in complex with RabGGTase β (GTPase_G:β-su) were added to the system to a final concentration of 2.5 μM in a total volume of 2 mL (50 mM Tris, pH 7.5, 300 mM NaCl, 5 mM $MgCl_2$, 1 mM Tris(2-carboxyethyl)phosphine, 0.1 mM GDP). Following the binding step, unbound protein was washed out of the system. GDI and $TBC1D20_{1–362}$ were used at 1 μM, and Lem3 at 100 nM concentration. The data points in the kinetics represent the normalized area of the amide II band (1,600–1,482 cm^{-1} integration range). For titrations with different concentration *c* of GDI, the system was allowed to reach equilibrium

between membrane-bound and dissociated Rab, and GDI was then added at increasing concentrations. The fraction of membrane-bound Rab (F) was normalized and fitted according to a logistic sigmoidal function (ref. 8; Eq. **S1**) to yield EC_{50} values for GDI-mediated membrane extraction:

$$F(c) = \frac{1}{1 + (c/EC_{50})^p}. \quad \textbf{[S1]}$$

The dephosphocholinase Lem3 acts on Rab1b but not on wild-type Rab35. Therefore, Rab35T76S, which is a substrate for Lem3, was used in the experiment shown in Fig. 5*A*. However, the titration in Fig. 5*B* was performed with wild-type Rab35.

Nucleotide exchange from GDP to GTP was performed before membrane binding by incubation of Rab35_G:β-su with 15 μM Connecdenn and 0.3 mM GTP for 1 h on ice and 10 min at room temperature. GDP was replaced by GTP in the buffer for the ATR experiment.

We compared membrane extraction by bovine GDI-1 to that of yeast GDI from *S. cerevisiae*. Yeast GDI possesses an even lower EC_{50} value for membrane extraction as bovine GDI-1 (Fig. S7). Therefore, yeast GDI is also a good model for the study of membrane extraction of mammalian Rab GTPases. Experiments shown in Figs. 3, 4, and 5*A* were done with yeast GDI, but all titrations (Fig. 5 and Figs. S4 and S7) were done with bovine GDI-1 to obtain EC_{50} values relevant for the mammalian system.

Difference spectra of the "off" to "on" transition of Rab35 were obtained by adding 4 mM BeF_2 and 16 mM NaF to the buffer.

Characterization of the Lipid Bilayer. The thin film weak absorber approximation was used to calculate the surface concentration and order parameters, as described elsewhere (7, 9, 10). All input parameters, derived parameters, and final parameters and their respective error margins are given in Table S1. Relevant equations are given below. Error analysis was performed using Gaussian error propagation.

Calculation of electrical field strengths E_x, E_y, and E_z (Eqs. **S2a**, **S2b**, and **S2c**) relative to the experimental coordinate system requires knowledge of the angle of incidence (θ) and the refractive indices of germanium (n_1), lipid (n_2), and water (n_3):

$$E_x = \frac{2\cos\theta\sqrt{\sin^2\theta - (n_3/n_1)^2}}{\sqrt{\left((1+(n_3/n_1)^2)\sin^2\theta - (n_3/n_1)^2\right)\left(1-(n_3/n_1)^2\right)}}, \quad \textbf{[S2a]}$$

$$E_y = \frac{2\cos\theta}{\sqrt{1-(n_3/n_1)^2}}, \quad \textbf{[S2b]}$$

$$E_z = \frac{(n_3/n_2)^2\sin 2\theta}{\sqrt{\left((1+(n_3/n_1)^2)\sin^2\theta - (n_3/n_1)^2\right)\left(1-(n_3/n_1)^2\right)}}. \quad \textbf{[S2c]}$$

Surface concentration Γ is calculated according to Eq. **S3** and requires input of E_x, E_y, E_z, integrated absorbances A_{pp} and A_{vp} of the band of interest [i.e., $\nu_{as}(CH_2)$], the integrated extinction coefficient ε of the group of interest, the number of these groups n_{Gr} per molecule (i.e., number of CH_2 groups in a lipid), and the number of active reflections N in the IRE. Due to the polarizer leak fraction f (11) obtained values for A_{pp} and A_{vp} need to be corrected according to Eqs. **S4a** and **S4b**, yielding A^{ideal} for pp and vp absorptions. Note that Eq. **S3** assumes isotropic distribution of the absorbing molecule and results in equal values obtained with parallel and vertical polarized light. For oriented samples, such as a lipid bilayer, different results are obtained:

$$\Gamma = \frac{\int A_{pp}^{ideal}(\tilde{\nu})\,\mathrm{d}\tilde{\nu}\,\frac{n_1}{n_2}\cos\theta}{\mathrm{n_{Gr}}N\int \varepsilon(\tilde{\nu})d\tilde{\nu}\left(E_x^2+E_z^2\right)} = \frac{\int A_{vp}^{ideal}(\tilde{\nu})\,\mathrm{d}\tilde{\nu}\,\frac{n_1}{n_2}\cos\theta}{\mathrm{n_{Gr}}N\int \varepsilon(\tilde{\nu})\,\mathrm{d}\tilde{\nu}E_y^2}, \quad \textbf{[S3]}$$

$$A_{pp}^{ideal} = \frac{A_{pp} - f\,A_{vp}^{ideal}}{1-f}, \quad \textbf{[S4a]}$$

$$A_{vp}^{ideal} = \frac{A_{vp} - f\,A_{pp}^{ideal}}{1-f}. \quad \textbf{[S4b]}$$

The experimental dichroic ratio R_{ATR} (Eq. **S5**) contains orientational information and allows calculation of the order parameter S (Eq. **S6**):

$$R_{ATR} = \frac{\int A_{pp}^{ideal}(\tilde{\nu})\,\mathrm{d}\tilde{\nu}}{\int A_{vp}^{ideal}(\tilde{\nu})\,\mathrm{d}\tilde{\nu}}, \quad \textbf{[S5]}$$

$$S = \frac{E_x^2 - R_{\mathrm{ATR}}E_y^2 + E_z^2}{E_x^2 - R_{\mathrm{ATR}}E_y^2 - 2E_z^2}. \quad \textbf{[S6]}$$

S describes the orientation of the transition dipole moment of the absorbing group relative to the IRE normal. S is composed of S_{membrane}, S_{molecule}, and S_{dipole}, describing the relative orientations of the membrane normal to the IRE, the molecule axis to the membrane normal, and the transition dipole moment to the molecule axis, respectively (Eq. **S7**):

$$S = S_{\mathrm{membrane}}S_{\mathrm{molecule}}S_{\mathrm{dipole}}. \quad \textbf{[S7]}$$

S_{membrane} is typically assumed to be 1. Usually, the parameter of interest is S_{molecule} and can be calculated with the knowledge of the angle α between the transition dipole moment and the molecule axis (Eq. **S8**):

$$S_{\mathrm{molecule}} = \frac{2S}{3\cos^2\alpha - 1}. \quad \textbf{[S8]}$$

Order parameters can be converted to respective angles with Eq. **S9**. In this case, β would correspond to the angle between the membrane normal and the molecule axis:

$$\beta = \arccos\sqrt{\frac{2S_{\mathrm{molecule}}+1}{3}}. \quad \textbf{[S9]}$$

Surface concentration of membrane-bound Rab35 was calculated in the same manner, and the values are also given in Table S1.

1. Oesterlin LK, Goody RS, Itzen A (2012) Posttranslational modifications of Rab proteins cause effective displacement of GDP dissociation inhibitor. *Proc Natl Acad Sci USA* 109(15):5621–5626.
2. Goody PR, et al. (2012) Reversible phosphocholination of Rab proteins by *Legionella pneumophila* effector proteins. *EMBO J* 31(7):1774–1784.
3. Wu Y-W, Tan K-T, Waldmann H, Goody RS, Alexandrov K (2007) Interaction analysis of prenylated Rab GTPase with Rab escort protein and GDP dissociation inhibitor explains the need for both regulators. *Proc Natl Acad Sci USA* 104(30):12294–12299.
4. Gavriljuk K, et al. (2012) Catalytic mechanism of a mammalian Rab·RabGAP complex in atomic detail. *Proc Natl Acad Sci USA* 109(52):21348–21353.

5. Rak A, et al. (2003) Structure of Rab GDP-dissociation inhibitor in complex with prenylated YPT1 GTPase. *Science* 302(5645):646–650.
6. Güldenhaupt J, et al. (2012) *N*-Ras forms dimers at POPC membranes. *Biophys J* 103(7): 1585–1593.
7. Kötting C, Güldenhaupt J, Gerwert K (2012) Time-resolved FTIR spectroscopy for monitoring protein dynamics exemplified by functional studies of Ras protein bound to a lipid bilayer. *Chem Phys* 396:72–83.
8. Lata S, Piehler J (2005) Stable and functional immobilization of histidine-tagged proteins via multivalent chelator headgroups on a molecular poly(ethylene glycol) brush. *Anal Chem* 77(4):1096–1105.
9. Tatulian SA (2003) Attenuated total reflection Fourier transform infrared spectroscopy: A method of choice for studying membrane proteins and lipids. *Biochemistry* 42(41):11898–11907.
10. Reiter G, et al. (2002) Interaction of a bacterial endotoxin with different surfaces investigated by in situ Fourier transform infrared attenuated total reflection spectroscopy. *Langmuir* 18(15):5761–5771.
11. Lórenz-Fonfría VA, Granell M, León X, Leblanc G, Padrós E (2009) In-plane and out-of-plane infrared difference spectroscopy unravels tilting of helices and structural changes in a membrane protein upon substrate binding. *J Am Chem Soc* 131(42): 15094–15095.

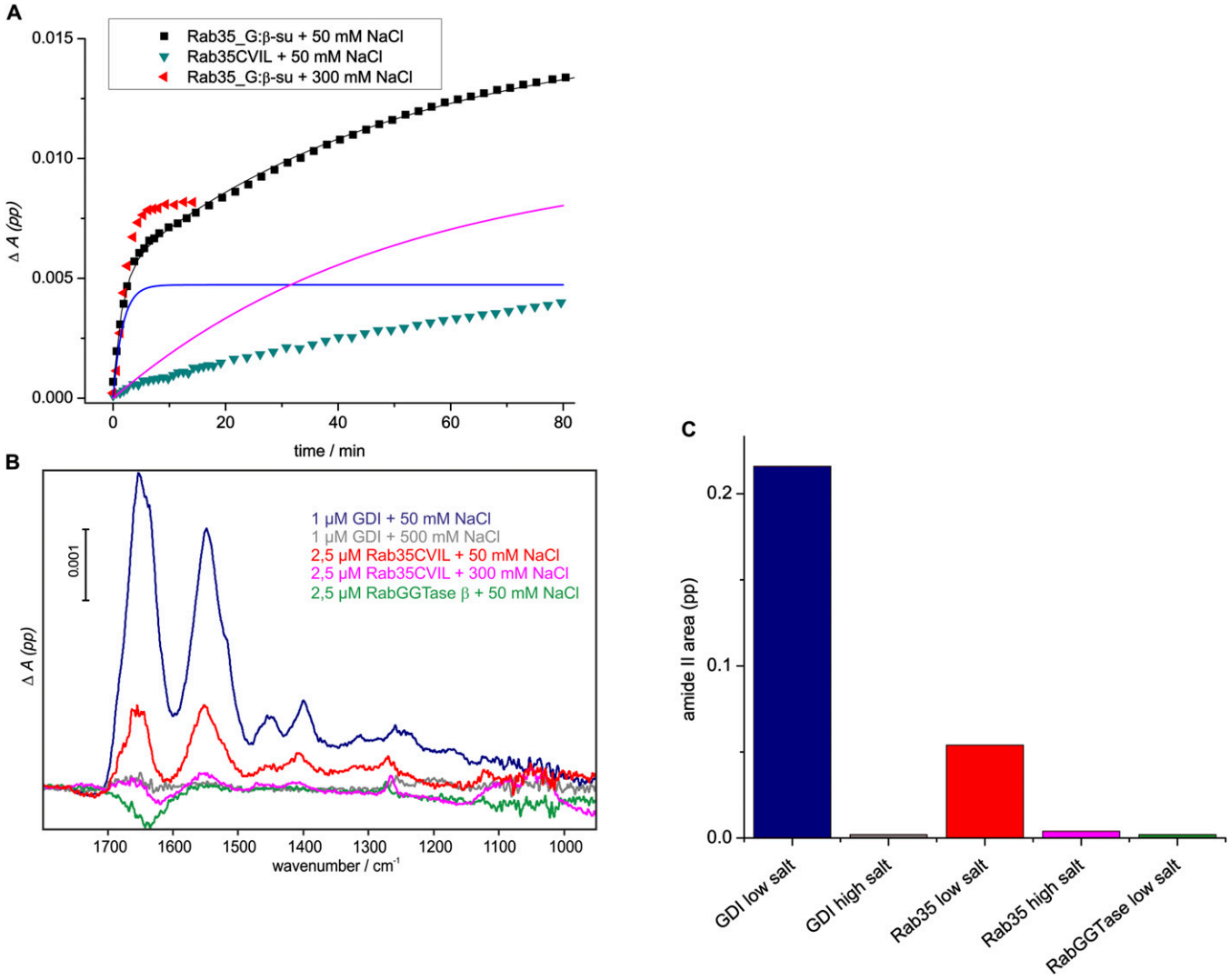

Fig. S1. Controls for nonspecific binding to the solid-supported DOPC/DOPS lipid bilayer. (*A*) Time course of Rab35 binding to the bilayer monitored at 1,548 cm^{-1} (height of the amide II band). Unprenylated Rab35 with the CAAX-box (Rab35CVIL) slowly but significantly binds to the negatively charged membrane in a nonspecific manner (cyan). This is also reflected in the biphasic binding of Rab35_G [black data points; two exponential fit components shown as blue (1.7 min^{-1}) and magenta (49 min^{-1}) lines; the sum is shown in black], where the slower component is due to the nonspecific binding. Raising the NaCl concentration to 300 mM abolishes the second nonspecific binding phase (red). β-su indicates that the GTPase is in complex with RabGGTase β. (*B*) Difference spectra (for clarity, only absorbance with parallel polarized light is shown) resulting after 20 min of circulation of different proteins over the membrane. GDI exhibits rather strong nonspecific binding at low salt concentrations (blue), which can be almost totally suppressed with 500 mM NaCl for 1 μM GDI (gray). Rab35CVIL also shows nonspecific binding (red) as already seen in Fig. S1*A*. This can be suppressed by 300 mM NaCl (magenta). RabGGTase β does not bind nonspecifically (green; the small negative band at ∼1,640 cm^{-1} is a water artifact). (*C*) Column diagram showing the amide II area of the spectra from *B*.

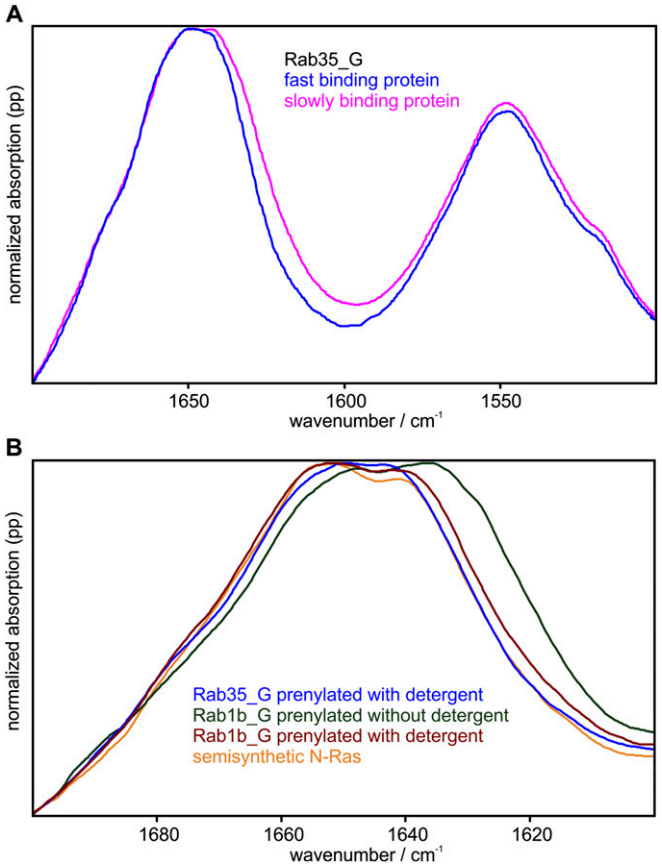

Fig. S2. Comparison of correctly folded and denatured proteins bound to the lipid bilayer. (*A*) Rab35_G binding fast or slowly (Fig. S1*A*) at low salt concentrations can be distinguished with the help of IR spectra. Slowly binding Rab35_G (magenta) possesses a significantly broader amide I band than fast binding Rab35_G (blue), indicating denaturation of the former. (*B*) Influence of detergent present during the prenylation reaction as seen in the amide I band of proteins bound to the membrane. Rab1b_G prenylated in the presence of RabGGTase β instead of detergent possesses a broader amide I band that is shifted to lower wave numbers (green) than does Rab1b_G prenylated with detergent (brown). The latter is also more similar to the amide I band of active Rab35_G (blue). Performing the prenylation in presence of detergent leads to better results. The amide I band of semisynthetic *N*-Ras is shown in orange as an example for a protein with the same fold that is known to be active on a solid-supported lipid bilayer [courtesy of J. Güldenhaupt (Department of Biophysics, Ruhr-University Bochum, Bochum, Germany); ref. 1].

1. Güldenhaupt J, et al. (2012) *N*-Ras forms dimers at POPC membranes. *Biophys J* 103(7):1585–1593.

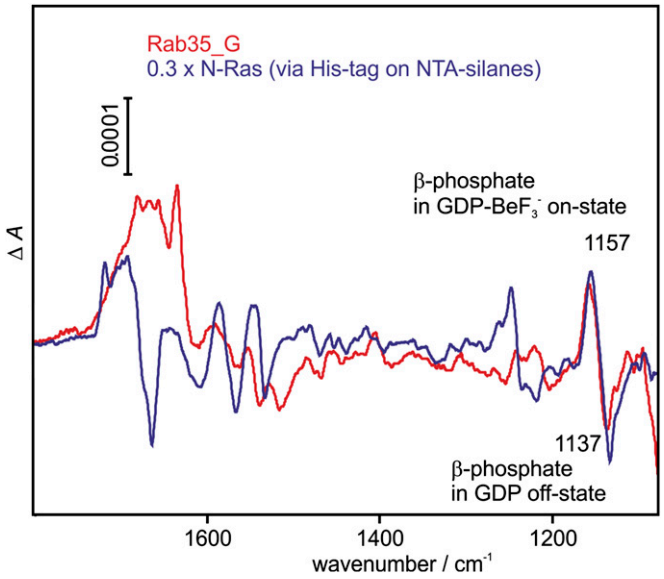

Fig. S3. Activity of membrane-bound Rab35_G shown by difference spectroscopy. BeF_3^- induces an "off" to "on" transition of Rab35_G·GDP, which is best seen at the β-phosphate bands of GDP at 1,157/1,137 cm^{-1}. These bands are present in the difference spectrum of Rab35 (red) as well as in the spectrum of *N*-Ras [blue; courtesy of J. Schartner (Department of Biophysics, Ruhr-University Bochum, Bochum Germany); ref. 1]. Notably, buffer artifacts are present in the spectrum of Rab35 because its dissociation from the membrane prevented titrations with BeF_3^- and subsequent multivariate curve resolution analysis, which eliminates such artifacts as in the spectrum of *N*-Ras.

1. Schartner J, et al. (2013) Universal method for protein immobilization on chemically functionalized germanium investigated by ATR-FTIR difference spectroscopy. *J Am Chem Soc* 135 (10):4079–4087.

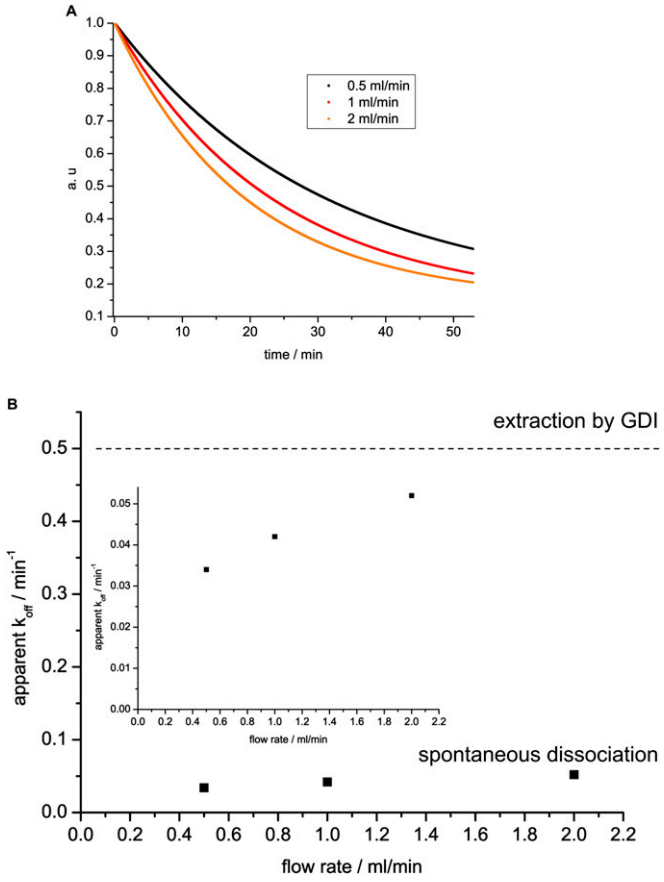

Fig. S4. Effect of rebinding and nucleotide dependency of the membrane extraction. (*A*) Flow rate increase during the wash step leads to higher apparent rate constants of membrane dissociation (0.034 min^{-1} at 0.5 mL/min, 0.042 min^{-1} at 1 mL/min, 0.052 min^{-1} at a flow rate of 2 mL/min) and indicates that rebinding effects are present. The volume above the germanium crystal is ∼0.5 mL and thus is exchanged four times per minute at 2 mL/min. Given the apparent rate constant of association (k_{on}) of Rab35_G with the membrane of 1.7 min^{-1}, binding is expected to interfere with the apparent dissociation rate constant (k_{off}) during the wash. (*B*) Plot of the apparent dissociation rate k_{off} against the flow rate, which shows that k_{off} moves toward saturation at higher flow rates (shown in *Inset*), as rebinding (due to k_{on}) is reduced. However, the observed extraction rate constant of GDI (Fig. 3) is at least an order of magnitude greater (dotted line). Therefore, the effect of GDI is not due to capturing of free Rab, but to an increase of k_{off}.

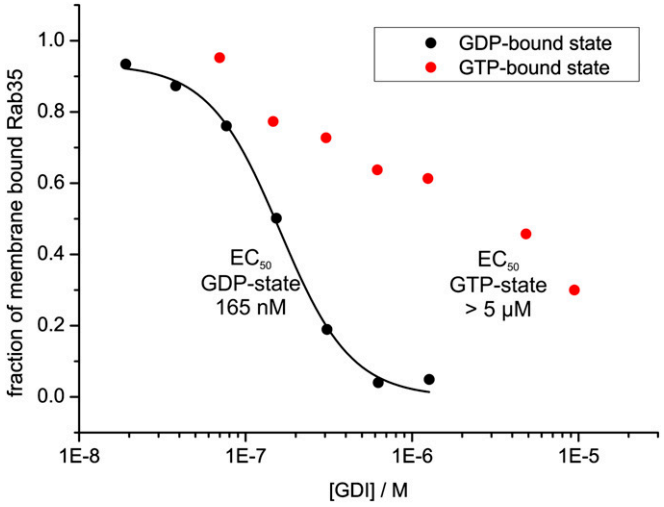

Fig. S5. Titration of membrane-bound Rab35_G with GDI in the GDP- and GTP-bound states. The data were fitted with a logistic sigmoidal function (*SI Materials and Methods*). The EC_{50} value for the extraction of Rab35_G in the GDP-state is 165 ± 5 nM. The data for the GTP-bound state seem to be composed of two curves and indicate that about 30% of the protein is in the GDP-bound state. The exact EC_{50} value for the GTP state could not be determined due to nonspecific binding of GDI to the membrane at high concentrations, but appears to be >5 µM.

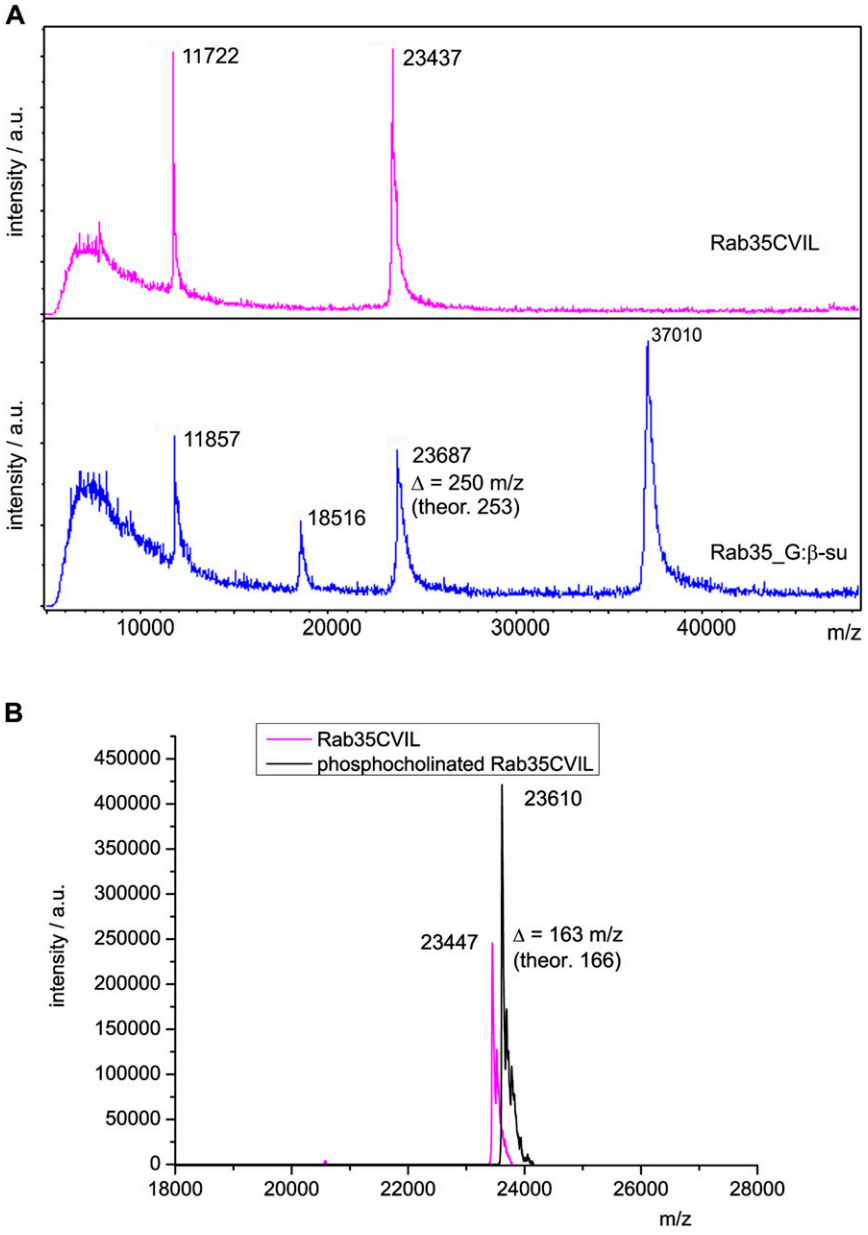

Fig. S6. (*A*) MALDI-MS spectra of unprenylated and geranylgeranylated Rab35. The measurements and data are courtesy of K. Kuhlmann and X. Liu (Medical Proteome Center, Ruhr-University Bochum, Bochum, Germany). Rab35CVIL (*Upper*) is detected as $[M+H]^+$ at 23,437 *m/z* (23,441 expected) and as $[M+2H]^{2+}$ at 11,722 *m/z*. Rab35_G (*Lower*) is detected as $[M+H]^+$ at 23,687 *m/z* (23,694 expected) and as $[M+2H]^{2+}$ at 11,857 *m/z*. The determined mass shift of 250 *m/z* agrees well with the expected shift of 253 *m/z* for geranylgeranylation. The error of ±3 *m/z* is well within accuracy of MALDI-MS. RabGGTase β present in the geranylgeranylated sample is detected at 37,010 and 18,516 *m/z*. (*B*) ESI-MS spectra of unmodified and phosphocholinated Rab35CVIL. Unmodified protein is detected at 23,447 *m/z* (23,441 expected), whereas phosphocholinated protein is detected at 23,610 *m/z* (23,607 expected). The determined mass shift of 163 *m/z* agrees well with the value of 166 expected for phosphocholination.

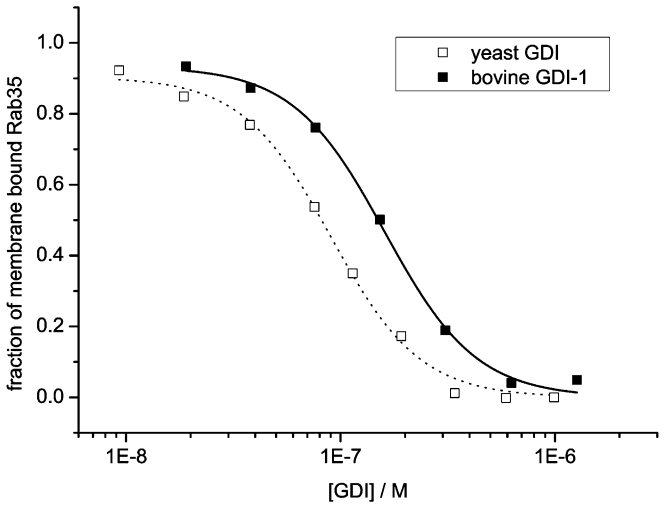

Fig. S7. Titration of membrane-bound Rab35_G with yeast GDI and bovine GDI-1. The data were fitted with a logistic sigmoidal function and yielded EC_{50} values of 90 and 165 nM for yeast GDI (open squares) and bovine GDI-1 (black squares), respectively. Yeast GDI behaves very similarly to bovine GDI-1 and is therefore a good model for interaction studies with mammalian Rab GTPases. It is even more effective at extracting membrane-bound Rab35 than its mammalian homolog.

Table S1. Parameters for the characterization of the lipid bilayer and the protein monolayer

Parameter	Value	Uncertainty	Source/comments
Primary input parameters			
Angle of incidence, θ	45	1.5	Refs. 1 and 2
Number of active reflections, *N*	12.5	0.5	Ref. 1
Refractive index of germanium, *n*1	4	0.005	Refs. 1–3
Refractive index of lipid/protein	1.44	0.05	Refs. 1–3; error set to 3%
Refractive index of water, *n*3	1.417 at 2,925 cm^{-1} 1.274 at 1,740 cm^{-1}	0.05	Refs. 2 and 3
Polarizer leak fraction	0.034		
Integrated extinction coefficient of a CH2 group (2,990–2,812 cm^{-1})	$4.71 \cdot 10^6$ cm/mol	$1.41 \cdot 10^3$	Ref. 3; error set to 3%
Number of CH2 groups *n*Gr in the acyl chains of DOPC/DOPS	28		
Angle α for CH2 groups	90°		Ref. 3
Angle α for CO groups	0°		Ref. 3
Integrated extinction coefficient of a peptide bond (1,600–1,485 cm^{-1})	10^7 cm/mol	$3 \cdot 10^5$	Ref. 3; error set to 3%
Number *n*Gr of peptide bonds in Rab35	204		
Derived parameters			
Ex at 2,925 cm^{-1}	1.39	0.034	
Ey at 2,925 cm^{-1}	1.51	0.04	
Ez at 2,925 cm^{-1}	1.58	0.17	
Ex at 1,740 cm^{-1}	1.40	0.035	
Ey at 1,740 cm^{-1}	1.49	0.039	
Ez at 1,740 cm^{-1}	1.24	0.14	
Calculated parameters			
Lipid surface concentration Γ	306/372 pmol/cm^2	46/37	*App*/*Avp* values, average value of 339 pmol/cm^2
Area per lipid in a bilayer	108/89 $Å^2$	16/9	*App*/*Avp* values, average value of 99 $Å^2$
Smolecule of the acyl chains	0.23	0.14	
Angle β between the acyl chains and the membrane normal	45	6	Average angle
Smolecule of the carbonyl groups	−0.21	0.08	
Angle β between the carbonyl groups and the membrane normal	64	4	Average angle, notably not the magic angle
Surface concentration Γ of membrane-bound Rab35 or Rab1b	4–6 pmol/cm^2		Variation is not due to calculation errors, but represents the range used in the experiments

1. Kötting C, Güldenhaupt J, Gerwert K (2012) Time-resolved FTIR spectroscopy for monitoring protein dynamics exemplified by functional studies of Ras protein bound to a lipid bilayer. *Chem Phys* 396:72–83.
2. Reiter G, et al. (2002) Interaction of a bacterial endotoxin with different surfaces investigated by in situ Fourier transform infrared attenuated total reflection spectroscopy. *Langmuir* 18(15):5761–5771.
3. Tatulian SA (2003) Attenuated total reflection Fourier transform infrared spectroscopy: A method of choice for studying membrane proteins and lipids. *Biochemistry* 42(41): 11898–11907.

Table S2. Kinetic parameters and EC_{50} values of the Rab–membrane/GDI interactions

Parameter	Value	Note
Apparent membrane association rate constant for Rab1b_G and Rab35_G	~1.7 min^{-1}	Not well separated from the mixing kinetics of the cell (Fig. 3, 4, or 5)
Apparent membrane dissociation rate constant for Rab35_G	0.034/0.042/0.052 min^{-1}	At flow rates of 0.5/1/2 mL/min (Fig. S4)
Apparent membrane dissociation rate constant for Rab1b_G	—	Not determined, several times larger than for Rab35_G (Fig. 4*A*)
Apparent rate constant for membrane extraction of Rab1b/35_G by GDI	>0.5 min^{-1}	Overlapping with/limited by exchange kinetics of the flow cell (Figs. 3 and 4)
EC50 value for membrane extraction of Rab35_G by bovine GDI-1	165 ± 5 nM	Fig. 5
EC50 value for membrane extraction of Rab35_G in the GTP-bound state by bovine GDI-1	>5 μM	Not determined due to nonspecific binding of GDI to the membrane (Fig. S5)
EC50 value for membrane extraction of phosphocholinated Rab35_G by bovine GDI-1	1.05 ± 0.05 μM	Fig. 5
EC50 value for membrane extraction of Rab35_G by yeast GDI	90 ± 5 nM	Fig. S7